IEEE Access
Multidisciplinary ⋮ Rapid Review ⋮ Open Access Journal

Received July 13, 2020, accepted July 23, 2020, date of publication July 28, 2020, date of current version August 10, 2020.

Digital Object Identifier 10.1109/ACCESS.2020.3012455

A Memristive Chaotic System With Hypermultistability and Its Application in Image Encryption

JIAYU SUN[1,2], CHUNBIAO LI[1,2], (Member, IEEE), TIANAI LU[1,2], AKIF AKGUL[3], (Member, IEEE), AND FUHONG MIN[4]

[1]Jiangsu Collaborative Innovation Center of Atmospheric Environment and Equipment Technology (CICAEET), Nanjing University of Information Science and Technology, Nanjing 210044, China
[2]Jiangsu Key Laboratory of Meteorological Observation and Information Processing, Nanjing University of Information Science and Technology, Nanjing 210044, China
[3]Department of Electrical and Electronics Engineering, Faculty of Technology, Sakarya University of Applied Sciences, 54187 Sakarya, Turkey
[4]School of Electrical and Automation Engineering, Nanjing Normal University, Nanjing 210023, China

Corresponding authors: Chunbiao Li (chunbiaolee@nuist.edu.cn) and Fuhong Min (minfuhong@njnu.edu.cn)

This work was supported in part by the National Natural Science Foundation of China under Grant 61871230 and Grant 61971228; in part by the Natural Science Foundation of Jiangsu Province under Grant BK20181410; and in part by the Project Funded by the Priority Academic Program Development of Jiangsu Higher Education Institutions.

ABSTRACT Infinite lines of equilibria exist in a new memristive system when a tangent function is introduced for attractor self-reproducing. Lyapunov exponent spectra and bifurcation diagram shows that the newly proposed chaotic system exhibits intermittent chaos and hypermultistability characterized for the coexistence of infinite countable and uncountable attractors. The physical feasibility of the new memristive chaotic system is confirmed by PSpice circuit simulation. Finally, the system is applied in color image encryption, where the performance in the process is evaluated. Numerical simulation proves that the new memristive chaotic system has high security in image encryption.

INDEX TERMS Memristive chaotic system, infinite lines of equilibria, image encryption.

I. INTRODUCTION

In recent years, memristor has been introduced into chaotic systems widely, which is used in neural networks [1]–[4], communication systems [5]–[7], computer engineering [8]–[10], chaotic signal control [11]–[15] and image encryption [16]–[19]. Studies of hidden attractors allow the understanding of potentially unexpected disastrous responses of dynamical systems to perturbations [20]–[22]. Therefore, increasing attention has been found to hidden oscillations of chaotic systems [23]–[26], and equilibrium point is one of the key factors influencing the dynamical characteristics in chaotic system. The number or type of equilibria shows its power in chaos producing or manifold complexity. Lorenz, Lorenz - like systems [27]–[29] and Chua systems [22], [30]–[34] have a couple of unstable equilibria [35], [36], while some other chaotic systems without any equilibria [37]–[39] or with infinite equilibria [40]–[43] shows different properties compared with the formers.

In general, systems with more equilibria may bring unexpected stabilities to some extent, such as extreme multistability [34], [44]–[46], megastability [47], [48] and infinite multistability [49], [50]. Extreme multistability is mainly associated with the memory effect from a memristor or from coupling. Megastability or infinite multistability is usually induced by periodic trigonometric function for initial-condition based offset boosting. To the best of our knowledge, there is no chaotic case found showing both extreme and infinite multistability, which forms the first motivation of this work. For better demonstration, we firstly define this multistability as hypermultistability for those cases hosting infinite countable and uncountable attractors different from extreme multistability, megastability and other conventional infinite multistability. Furthermore, chaotic systems have been applied for image encryption. In [51], a new three-dimensional chaotic system without equilibria

The associate editor coordinating the review of this manuscript and approving it for publication was Sun Junwei.

is presented and its real environment electronic circuit is designed and implemented, and applied to chaotic image encryption. In [52], a new chaotic system with infinite number of equilibria located on an exponential curve is presented, the new random number generator and encryption algorithm are designed. In [53], a multi-vortex chaotic system based on simplified Lorenz system with unstable equilibria is designed and applied to chaotic image encryption. These explorations show the possibility for chaos-based application. However, there is no chaotic system with infinite lines of equilibria and hypermultistability applied in image encryption.

In this paper, a new memristive chaotic system with infinite lines of equilibria and hypermultistability is designed for application in image encryption. In section 2, the model of the memristive chaotic system is given with basic analysis. In section 3, bifurcation analysis finds the inherent intermittent chaos. In section 4, hypermultistability is observed by two initial-value-triggered regimes of bifurcation. In section 5, an analog circuit experiment is completed by PSpice simulation for system verification. In section 6, the chaotic sequence generated by the new system is applied into image encryption. Conclusion is drawn in the last section.

II. SYSTEM MODEL

Based on the chaotic system variable boostable VB2 [54], which has only one quadratic term and four linear terms, a new memristive chaotic system is obtained by inserting tangent functions and a memristor,

$$\begin{cases} \dot{x} = y + y\tan(z), \\ \dot{y} = -\tan(z), \\ \dot{z} = xW(u) - a\tan(z), \\ \dot{u} = x. \end{cases} \tag{1}$$

where the flux-controlled memductance is $W(u) = b|u| - c$ is introduced in the third dimension.

Here the flux-controlled memristor is defined as,

$$\begin{cases} i = W(u)x, \\ W(u) = b\,|u| - c, \\ \dot{u} = x. \end{cases} \tag{2}$$

The flux-controlled memductance is related to the system variable x, which can be written as,

$$W(u) = b\,|u| - c = b\left|\int_{-\infty}^{t} x ds\right| - c = bW_0 + b\left|\int_{0}^{t} x ds\right| - c \tag{3}$$

where $W(u) = \left|\int_{-\infty}^{t} x ds\right| - \left|\int_{0}^{t} x ds\right|$.

The plot of memductance and pinched hysteresis curve are shown in Fig. 1.

System parameters are chosen as $a = 1$, $b = 2$, $c = 2$ and four attractors appear in different positions, as shown in Fig. 2, which have the same Lyapunov exponents (0.9801, 0, −1.3328, −5.683) and Kaplan-Yorke dimension of 2.7354.

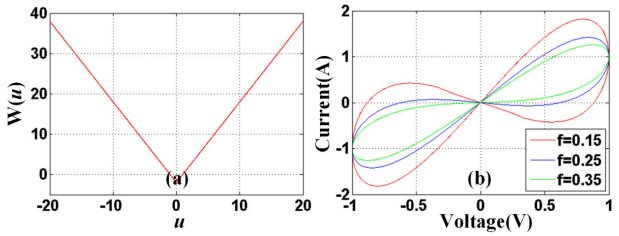

FIGURE 1. The memductance and pinched hysteresis loop.

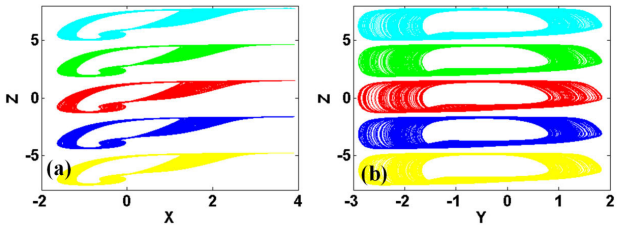

FIGURE 2. Coexisting chaotic attractors of system (1) with $a = 1$, $b = 2$, $c = 2$, [0, 1, 0, 0] is red, [0, 1, π, 0] is green, [0, 1, $-\pi$, 0] is blue, [0, 1, 2π, 0] is cyan, [0, 1, -2π, 0] is yellow: (a) x - z plane, (b) y - z plane.

III. BASIC DYNAMICAL ANALYSIS

A. ANALYSIS OF EQUILIBRIA AND STABILITY

Let $-\tan(z) = 0$, it is easy to calculate the solution z ($z = k\pi$) ($k \in$N). When $a = 1$, $b = 2$, $c = 2$, system (1) has infinite equilibria $(0, 0, k\pi, u)(k \in \mathrm{N})$, the characteristic polynomial equation is,

$$\lambda(\lambda^3 + a\lambda^2 - c + b\,|u|) = 0 \tag{4}$$

Considering Routh–Hurwitz condition are given by,

$$\begin{cases} a > 0, \\ W(u) > 0, \\ a \cdot 0 - W(u) > 0. \end{cases} \tag{5}$$

When the parameters of the system (1) are all positive, it is found that Routh-Hurwitz condition is not satisfied. When $a = 1$, $b = 2$, $c = 2$, the eigenvalues of the infinite lines equilibria have a pair of complex conjugate roots with positive real parts, demonstrating that the infinite lines equilibria is an unstable saddle point.

B. BIFURCATION ANALYSIS

When the parameter a varies in [0.5, 2], intermittent chaos is found in system (1) where chaos and periodic oscillation appear alternately as shown in Fig. 3. As can be seen from the figure, when a is in the interval [0.55, 0.65] and [1.7, 2], the system produces cycle-1 attractor. When a is in the interval [0.5, 0.55] and [1.2, 1.7], the system produces cycle-2 attractors. When a is in the interval [0.82, 0.95], the system produces cycle-3 attractors. When a is in the interval [1.13,1.2], the system produces cycle-4 attractors.

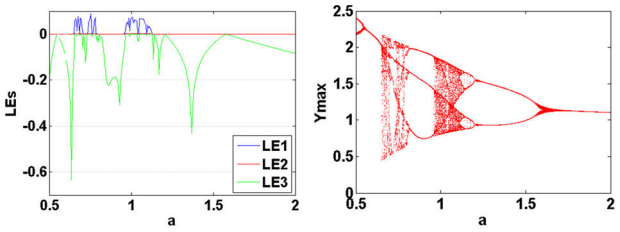

FIGURE 3. Lyapunov exponents and bifurcation diagram of system (1) with $b = 2$, $c = 2$, when a varies in [0.5, 2].

When a is in the interval [0.65, 0.82] and [0.95, 1.13], system in a state of chaos. Typical phase portraits of attractors of system (1) under different parameters are shown in Fig. 4. The corresponding Lyapunov exponents are shown in Table 1.

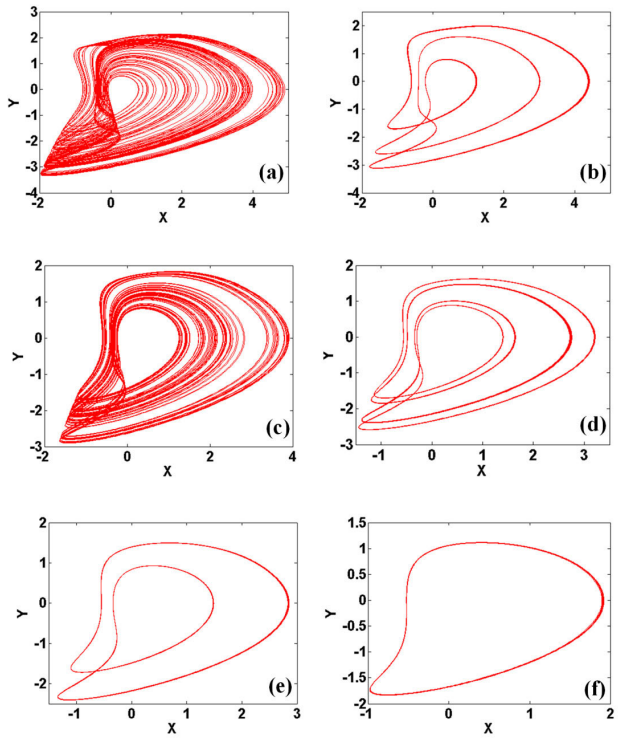

FIGURE 4. Phase portraits of attractors of system (1) with $b = 2$, $c = 2$ and IC = (0, 1, 0, 0) on the x - y plane: (a) $a = 0.69$, (b) $a = 0.86$, (c) $a = 1.0$, (d) $a = 1.18$, (e) $a = 1.3$, (f) $a = 1.9$.

When fixing $a = 1$ and $c = 2$ and the parameter b changes in the interval [1], [3], the Lyapunov exponents and Bifurcation diagram of system (1) are shown in Fig. 5, which can be seen from the figure. When the value of b is in the interval [1, 1.16], the system is in a chaotic state; when the value of b is in the interval [1.16, 1.73], the system is in a periodic state; when the value of b is in the interval [1.73, 3], the system returns to chaotic state.

When the fixed $a = 1$ and $b = 2$ and the parameter c changes in the interval [1, 3], the Lyapunov exponents and Bifurcation diagram of system (1) are shown in Fig. 6. It can be seen from the figure that when the value of c is

TABLE 1. Attractors in system (1) with $b = 2$, $c = 2$ under initial conditions of [0, 1, 0, 0].

Attractor	Parameter	LEs	D_{KY}
chaos	$a = 0.69$	(0.0147, 0, -0.0011, -7.2068)	3.0020
cycle-3	$a = 0.86$	(0, 0, -0.2302, -6.7454)	1
chaos	$a = 1.00$	(0.9801, 0, -1.3328, -5.683)	2.7354
cycle-4	$a = 1.18$	(0, 0, -0.0485, -5.9043)	1
cycle-2	$a = 1.30$	(0, 0, -0.0919, -5.7868)	1
cycle-1	$a = 1.90$	(0, 0, -0.0653, -5.7825)	1

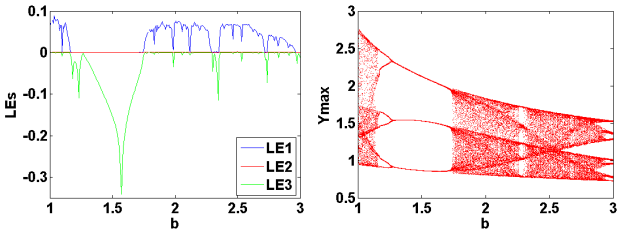

FIGURE 5. Lyapunov exponents and bifurcation diagram of system (1) with $a = 1$, $c = 2$, when b varies in [1, 3].

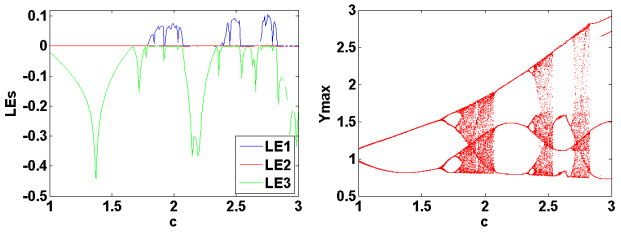

FIGURE 6. Lyapunov exponents and bifurcation diagram of system (1) with $a = 1$, $b = 2$, when c varies in [1, 3].

in the interval [1, 1.63], the system is in the cycle-2 state; when the value of c is in the interval [1.63, 1.75], the system is in the cycle-4 state. When the value is in the interval [1.75, 2], the system is in a chaotic state; when the value of c is in the interval [2, 2.3], the system is in the cycle-3 state, when the value of c is in the interval [2.3, 2.83], The system is in a chaotic state, and when the value of c is in the interval [2.83, 3], The system is in a periodic state.

IV. MULTISTABILITY ANALYSIS

In general, the value of a memristor has some relations with the initial condition. When the initial condition u_0 varies in $[-2, 2]$, the system has different stable state, in which Lyapunov exponent and bifurcation evolution are shown in Fig. 7, where the typical phase portraits of attractors under different u_0 are shown in Fig. 8. The corresponding Lyapunov exponents are shown in Table 2.When the initial condition z_0 varies in $[-1, 1]$, the system has different stable states, indicated by Lyapunov exponents and bifurcation diagram

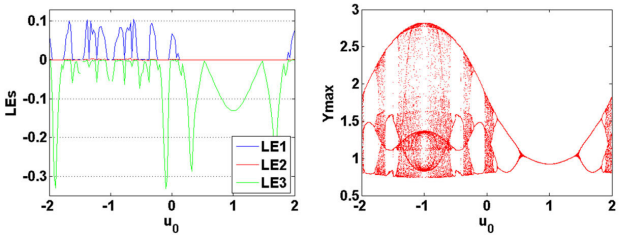

FIGURE 7. Dynamical behavior of system (1) with $a = 1$, $b = 2$, $c = 2$ under initial condition [0, 1, 0, u_0]: (a) Lyapunov exponents, (b) bifurcation diagram.

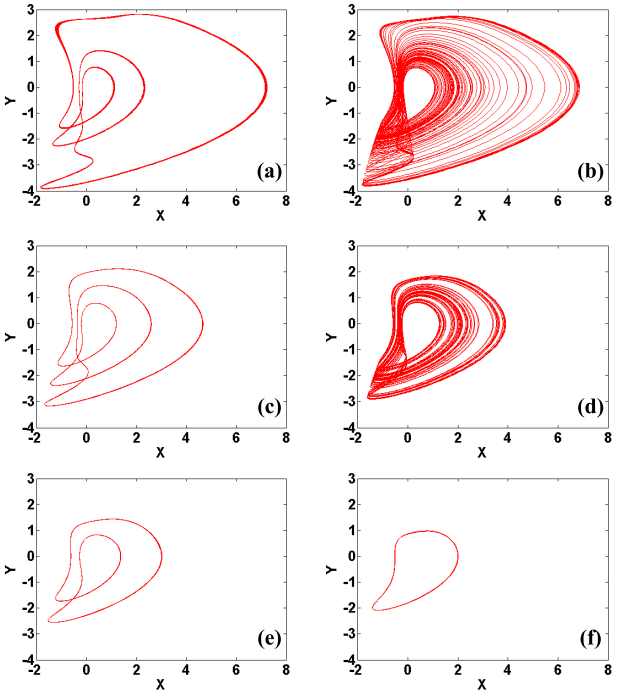

FIGURE 8. Coexisting attractors of system (1) with $a = 1$, $b = 2$, $c = 2$ under the initial condition [0, 1, 0, u_0]: (a) $u_0 = -1$, (b) $u_0 = -0.65$, (c) $u_0 = -0.15$, (d) $u_0 = 0$, (e) $u_0 = 0.25$, (f) $u_0 = 0.7$.

shown in Fig. 9, where the typical phase portraits of attractors under different z_0 are shown in Fig. 10. The corresponding Lyapunov exponents are shown in Table 3.

The property of multistability is unique. From Fig. 7 and Fig. 9, intermittent chaos with small interval and large interval are captured. Furthermore, for the periodic tangent function, all the infinite countless attractors can be self-reproduced as shown in Fig. 11. All the periodic or chaotic attractors are reproduced in the dimension of z. Here the unique hypermultistability is clearly seen in phase space. Here four typical attractors including chaos and limit cycles are reproduced in phase space for clear demonstration.

V. CIRCUIT IMPLEMENTATION

When $a = 1$, $b = 2$, $c = 2$ and under different initial conditions, we find that the system variables oscillate between -15 and 15 from the Fig. 2. Therefore, it is convenience for circuit design from the original equation by using the operational amplifier OPA404, the ideal multiplier, the diode D1N4500 and the tan operation unit. The analog

TABLE 2. Attractors in system (1) with $a = 1$, $b = 2$, $c = 2$ under initial conditions of [0, 1, 0, u_0].

Attractor	Initial condition	LEs	D_{KY}
cycle-3	$u_0 = -1$	(0, 0, −0.0548, −8.4077)	1
chaos	$u_0 = -0.65$	(0.4688, 0, −0.5972,−7.4693)	2.7851
cycle-3	$u_0 = -0.15$	(0, 0, −0.1129, −7.4883)	1
chaos	$u_0 = 0$	(0.9801, 0, −1.3328,−5.6830)	2.7354
cycle-2	$u_0 = 0.25$	(0, 0, −0.1047, −4.9422)	1
cycle-1	$u_0 = 0.7$	(0, 0, −0.1759, −7.9140)	1

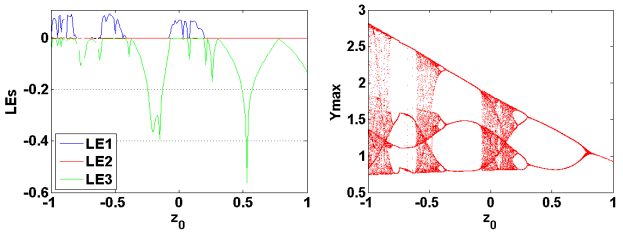

FIGURE 9. Dynamical behavior of system (1) with $a = 1$, $b = 2$, $c = 2$ under initial condition [0, 1, z_0, 0]: (a) Lyapunov exponents, (b) bifurcation diagram.

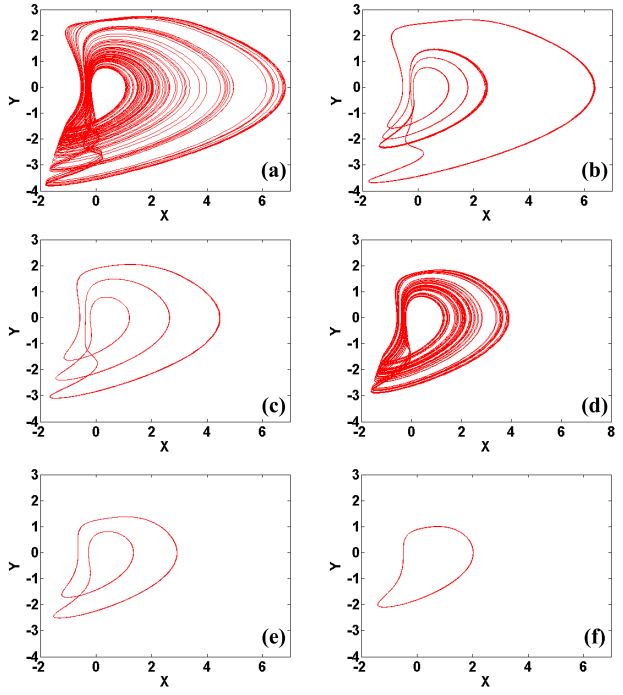

FIGURE 10. Coexisting attractors of system (1) with $a = 1$, $b = 2$, $c = 2$ under the initial condition [0, 1, z_0, 0]: (a) $z_0 = -0.9$, (b) $z_0 = -0.75$, (c) $z_0 = -0.2$, (d) $z_0 = 0$, (e) $z_0 = 0.5$, (f) $z_0 = 0.85$.

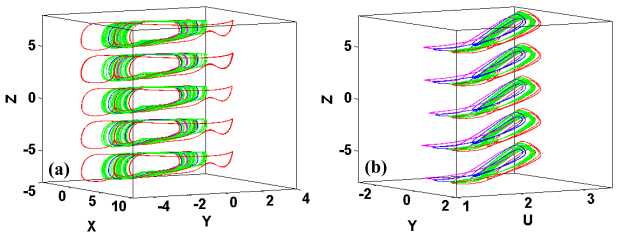

FIGURE 11. Coexisting attractors of system (1) with a = 1, b = 2, c = 2, [0, 1, 0/±π/±2π, 0] is green (chaos), [0, 1, 0/±π/±2π, −1] is red (cycle-3), [0, 1, 0/±π/±2π, 0.25] is blue (cycle-2), [0, 1, 0/±π/±2π, 0.7] is pink (cycle-1): (a) x - y - z space, (b) y - z - u space.

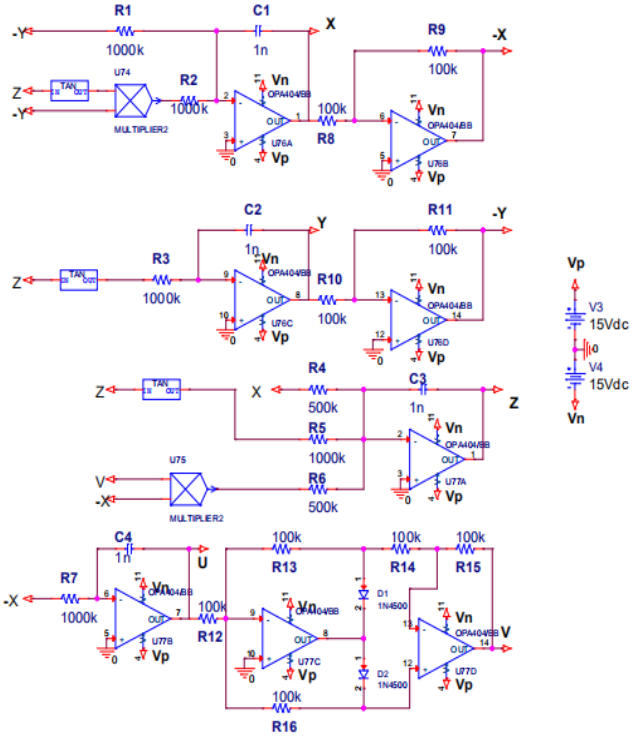

FIGURE 12. Circuit schematic of memristive system (1).

circuit is designed in PSpice as shown in Fig. 12 with the following circuit equation,

$$\begin{cases} \dot{x} = \dfrac{1}{R_1 C_1} y + \dfrac{1}{R_2 C_1} y \tan(z), \\ \dot{y} = -\dfrac{1}{R_3 C_2} \tan(z), \\ \dot{z} = -\dfrac{c}{R_4 C_3} x - \dfrac{a}{R_5 C_3} \tan(z) + \dfrac{b}{R_6 C_3} x\,|u|, \\ \dot{u} = \dfrac{1}{R_7 C_4} x. \end{cases} \tag{6}$$

Being equivalent with the combination of system parameter $a = 1$, $b = 2$, $c = 2$, circuit component parameters are selected as: $R_4 = R_6 = 500\text{k}\Omega$, $R_1 = R_2 = R_3 = R_5 = R_7 = 1000\text{k}\Omega$, $R_8 = R_9 = R_{10} = R_{11} = R_{12} = R_{13} = R_{14} = R_{15} = R_{16} = 100\text{k}\Omega$. Select capacitor $C_1 = C_2 = C_3 = C_4 = 1\text{nF}$. V represents $|u|$. Select initial

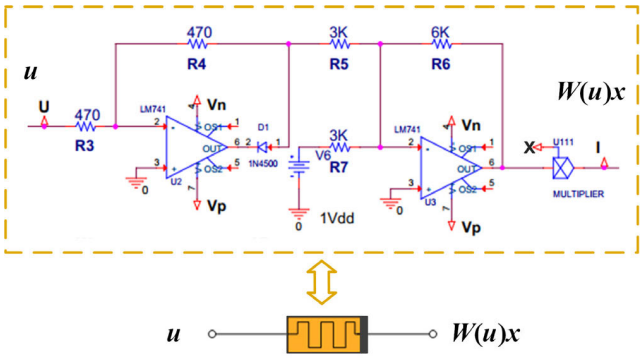

FIGURE 13. Equivalent circuit of the flux-controlled memristor.

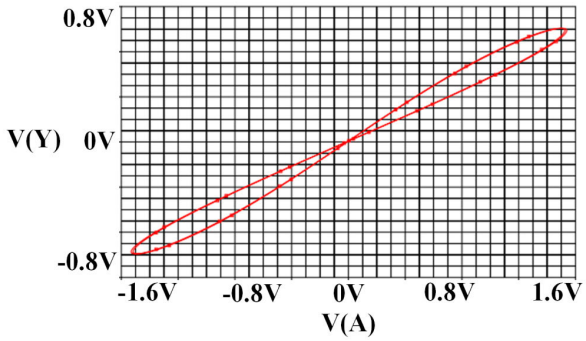

FIGURE 14. Pinched hysteresis loop of memristor W(*u*). (*x*-axis: 0.1v/div, *y*-axis: 0.1v/div).

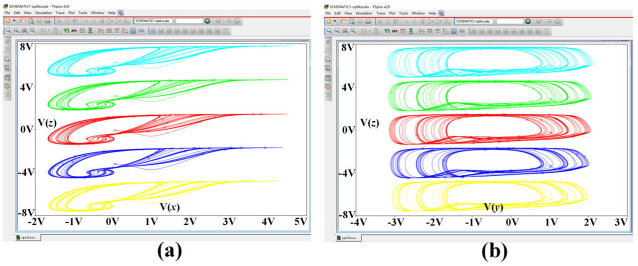

FIGURE 15. When $a = 1$, $b = 2$, $c = 2$, the system (1) takes chaotic attractors with different initial values. [0, 1, 0, 0], [0, 1, π, 0], [0, 1, −π, 0], [0, 1, 2π, 0], [0, 1, −2π, 0] are for red, green, blue, cyan, yellow correspondingly: (a) *x* – *z* plane, (b) *y* - *z* plane.

voltage of the capacitor $V_1 = V_3 = V_4 = 0\text{V}$, $V_2 = 1\text{V}$. In the following we select a tangent signal generator to reproduce the coexisting attractors. The circuit simulation diagram and a plot of pinched hysteresis loop of memristor are shown in Fig. 13 and Fig. 14. The chaotic attractor is shown in Fig. 15. The typical phase portraits of attractors under different u_0 are shown in Fig. 16., while the typical phase trajectories under different z_0 are indicated in Fig. 17.

VI. APPLICATION IN IMAGE ENCRYPTION

In contrast, the memristive chaotic system with infinite line equilibria has stronger unpredictability, larger key space and higher complexity, which makes the encryption more secure in theory.

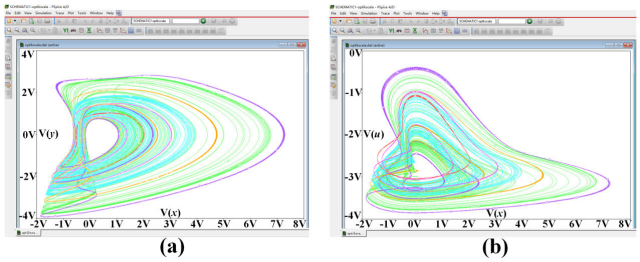

FIGURE 16. When $a = 1$, $b = 2$, $c = 2$, the system (1) takes attractors with different initial values. [0, 1, 0, −1], [0, 1, 0, −0.65], [0, 1, 0, −0.15], [0, 1, 0, 0], [0, 1, 0, 0.25], [0, 1, 0, 0.7] are for purple, green, orange, cyan, pink, red correspondingly: (a) x - y plane, (b) x - u plane.

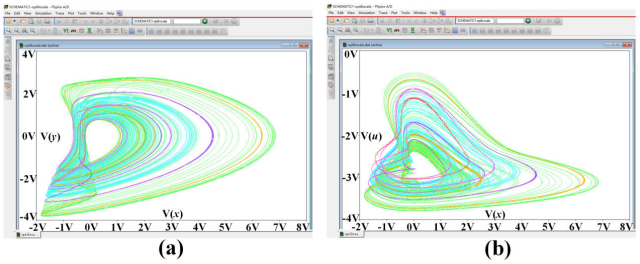

FIGURE 17. When $a = 1$, $b = 2$, $c = 2$, the system (1) takes attractors with different initial values. [0, 1, −0.9, 0], [0, 1, −0.75, 0], [0, 1, −0.2, 0], [0, 1, 0, 0], [0, 1, 0.5, 0], [0, 1, 0.85, 0] are for green, orange, purple, cyan, pink, red correspondingly: (a) x - y plane, (b) x - u plane.

A. ALGORITHM DESCRIPTION

In this paper, a method based on the combination of memristive chaotic system and DNA coding is used into encrypting the image. Here traditional DNA cryptography is applied for digital images encryption based on the chaotic sequences from a newly developed system. Compared with other algorithms, large space of encryption key and strong sensitivity is still found showing robustness against attacks. Its main contents include: firstly, the image is scrambled by Logistic chaotic mapping, and then the image is encrypted by combining DNA coding and computing with ordered random columns generated by memristive system. The specific encryption process is shown in Fig. 18.

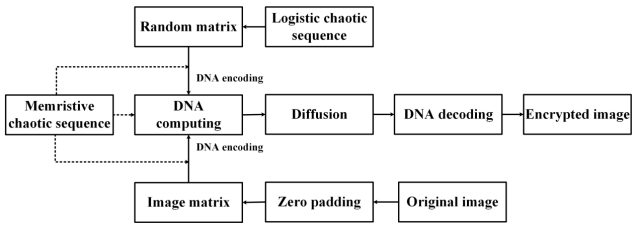

FIGURE 18. Encryption flowchart.

The specific encryption process is as follows:

Step1: In order to increase the applicability of the algorithm, the number of rows and columns of the image is supplemented into numbers that are divisible by t, which is the size of the block. Let the gray value of the filled pixel point M_0 and N_0 be 0;

Step2: Set the initial value x_0 and parameter μ of the Logistic mapping, and continuously iterate the Logistic mapping to obtain the one-dimensional sequence $\{p_i\}$ with length M × N + 1000 ($i = 1001, 1002..., M \times N + 1000$);

Step3: Convert all elements in the sequence into [0, 255], and then convert the sequence into a two-dimensional random matrix R of order M × N;

Step4: For the image and the random matrix, the size of each block is set as $t \times t$, where t is 4;

Step5: Four initial values X_0, Y_0, Z_0 and U_0 of the hypermultistability chaotic system were set, and four chaotic sequences, namely $\{x_i\}$, $\{y_i\}$, $\{z_i\}$ and $\{u_i\}$ ($i = 3002, 3003, \ldots, 3001 + M/t + N/t$);

Step6: $\{x_i\}$ and $\{y_i\}$ determine the DNA encoding mode of each block of image matrix and random matrix respectively. Taking image matrix as an example, the selection process of encoding mode is as follows: transform all elements in $\{x_i\}$,

$$x_i = \mathrm{mod}(\mathrm{round}(x_i \times 10^4), 8) + 1 \tag{7}$$

The gray value of all pixels in the block is converted into binary number and DNA coding is carried out in the x_i way;

Step7: $\{z_i\}$ determines the DNA operation between image matrix and random matrix. The selection process of DNA operation is as follows: transform all elements in $\{z_i\}$,

$$z_i = \mathrm{mod}(\mathrm{round}(z_i \times 10^4), 4) \tag{8}$$

If $z_i = 0$, DNA addition is performed between the ith block of image matrix and all corresponding pixels in the ith block of random matrix. If $z_i = 1$, it is a subtraction operation; If $z_i = 2$, is an xor operation; If $z_i = 3$, it is the same or operation;

Step8: In order to obtain better encryption effect, diffusion algorithm is introduced. The relationship between the current image block encryption result and the previous image block encryption result is also determined by $\{z_i\}$. Take $z_i = 0$ as an example, the encryption result c_i of the ith block is

$$c_i = c_{i-1} + I_i + R_i \tag{9}$$

The encrypted image is obtained after decoding.

Decryption algorithm is the inverse process of encryption algorithm. Random matrix and DNA encoding operation mode can be obtained through the key.

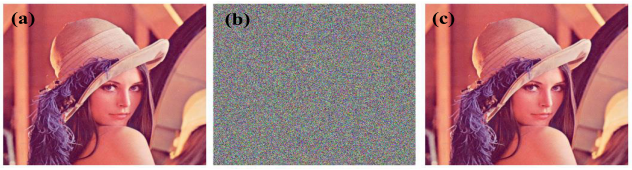

FIGURE 19. Encrypting experimental images: (a)the original image, (b)encrypted image, (c)decrypted image.

B. ENCRYPTION APPLICATION WITH MEMRISTIVE CHAOTIC SYSTEM AND DNA CODING

A standard color image is selected for testing, as shown in Fig. 19(a). The control parameters and initial conditions

TABLE 3. Attractors in system (1) with $a = 1$, $b = 2$, $c = 2$ under initial conditions of [0, 1, z_0, 0].

Attractor	Initial condition	LEs	D_{KY}
chaos	$z_0 = -0.9$	(0.0307, 0, −0.0908,−8.2225)	2.3349
cycle-4	$z_0 = -0.75$	(0, 0, -0.0347, −7.9390)	1
cycle-3	$z_0 = -0.2$	(0, 0, −0.3624, −6.9772)	1
chaos	$z_0 = 0$	(0.9801, 0, −1.3328,−5.6830)	2.7354
cycle-2	$z_0 = 0.5$	(0, 0, −0.0736, −5.1187)	1
cycle-1	$z_0 = 0.85$	(0, 0, −0.0425, −4.2898)	1

TABLE 4. Algorithm key.

Key	μ	x_0	X_0	Y_0	Z_0	U_0
Value	3.9999	0.5475	0	1	0	0
Key	k_1	k_2	M_0	N_0		
Value	0.3883	0.4134	0	0		

of the Logistic system are $\mu = 3.9999$ and $x_0 = 0.5475$, respectively. The system parameters of the new memristive chaotic system (1) are $a = 1$, $b = 2$ and $c = 2$. The initial conditions are set as $X_0 = 0$, $Y_0 = 1$, $Z_0 = 0$ and $U_0 = 0$. DNA coding rules are randomly generated. The selected keys are shown in Table 4. M_0 and N_0 are the parameters of zeroing during encryption; k_1 is the average gray level of channel G in the original image; k_2 is the average gray level of channel B in the original image. The encrypted image after simulation is shown in Fig. 19(b). It can be seen that the image after encryption is chaotic and completely different from the image before processing. Fig. 19(c) is the properly decrypted image, which is exactly the same as the original image.

C. SECURITY ANALYSIS

The most basic and immediate requirement for an encrypted system is security. Generally speaking, the chaotic image encryption system needs to have a large enough key space, reversible encryption and decryption, strong anti-attack and other performances, and then the performance of the chaos-based encryption will be analyzed from these aspects: key space analysis, histogram analysis, information entropy analysis, correlation analysis and analysis of anti-noise interference ability.

1) KEY SPACE ANALYSIS

With 64-bit computers, floating point precision up to 10^{-16}, the key space can reach $(10^{16})^{10} = 10^{160}$, which is larger than 10^{98} [19], so the new system can better resist the attacker's exhaustive attack. When the algorithm key is slightly changed, such as changing the key X_0 to 0.0000000000000001 with the other parameters unchanged, the decrypted image cannot be obtained correctly, as shown in Fig. 20. Therefore, the new system has strong key sensitivity.

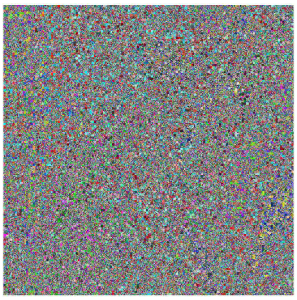

FIGURE 20. Initial condition perturbation ciphertext.

2) HISTOGRAM ANALYSIS

Gray histogram is a statistical analysis method, which can visually display the frequency distribution of each gray level pixel. After encryption, the histogram of the image becomes smooth and even from the fluctuation before encryption, so as to effectively prevent the attacker from obtaining the original image information by statistical analysis, resulting in information leakage, and ensure information security. Fig. 21(a) is the histogram of the original image, and (b) is the histogram of the encrypted image. It can be seen that the new system can resist a stronger attack.

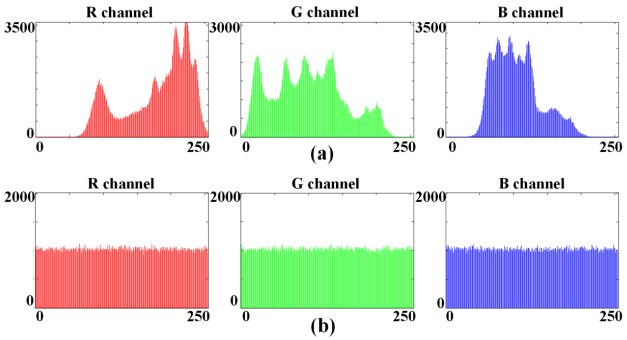

FIGURE 21. Encryption experiment histogram: (a)Histogram of the original image, (b)Encrypted image histogram.

3) INFORMATION ENTROPY ANALYSIS

Information entropy reflects the uncertainty of image information. The higher the entropy, the stronger the randomness. The random distribution of pixel values in image encryption is calculated as follows [17],

$$H(x) = -\sum_{i=1}^{N} p(x_i) \log_2 p(x_i) \tag{10}$$

where N represents the number of gray levels, x_i represents the gray level of the image, and $p(x_i)$ represents the frequency of the gray level. Theoretically, for a completely random digital image with a grayscale of 256, its pixel value is evenly distributed in [0, 255], then $p(x_i) = 1/256$ ($i \in [0, 255]$), and the calculated information entropy is 8bits. Therefore, if the image is encrypted, the closer the information entropy of the ciphertext image is to 8, the better the encryption

characteristics are. The information entropy of the three channel in original image and encrypted image by the system (1) are shown in Table 5, the entropy values obtained by our algorithm are larger than those of Ref. [18], which represents the great image encryption effect.

TABLE 5. Three-channel image information entropy in original and encrypted pictures.

Image	Red	Green	Blue
Original image	7.2682	7.5901	6.9951
Encrypted image	7.9992	7.9994	7.9994

4) CORRELATION ANALYSIS

The larger the correlation coefficient of adjacent pixels, the higher the correlation degree of adjacent pixels. Conversely, the smaller the coefficient, the lower the correlation. Therefore, the security of the algorithm can be judged by calculating the correlation coefficient. The smaller the coefficient, the lower the correlation and the higher the security. In order to measure the correlation between the original image and adjacent pixels of the ciphertext image, N pairs of adjacent pixels were selected from the image and the correlation coefficients were calculated from three directions: horizontal, vertical and diagonal. The correlation coefficients were calculated as follows [17],

$$E(x) = \frac{1}{N}\sum_{i=1}^{N} x_i \tag{11}$$

$$D(x) = \frac{1}{N}\sum_{i=1}^{N} (x_i - E(x))^2 \tag{12}$$

$$\mathrm{cov}(x, y) = \frac{1}{N}\sum_{i=1}^{N} (x_i - E(x))(y_i - E(y)) \tag{13}$$

$$r_{xy} = \frac{\mathrm{cov}(x, y)}{\sqrt{D(x)D(y)}} \tag{14}$$

where $\mathrm{cov}(x, y)$ represents correlation function and $D(x)$ represents mean square deviation.

TABLE 6. Correlation coefficient test results.

Image	Channel	horizontal	Vertical	Diagonal
Original image	Red	0.9749	0.9866	0.9623
	Green	0.9753	0.9873	0.9638
	Blue	0.9517	0.9711	0.9293
Encrypted image	Red	0.0007	0.0118	0.0154
	Green	0.0086	-0.0154	-0.0166
	Blue	0.0012	0.0014	0.0124

Table 6 shows the test results of the correlation coefficients of the adjacent pixels of the test image in various directions.

As can be seen from Table 6, the correlation coefficients of the original image are all close to 1, and the correlation coefficients of the encrypted image are all close to 0, indicating that the pixel point distribution of the encrypted image is highly discrete.

5) ANALYSIS OF ANTI-NOISE INTERFERENCE ABILITY

In the real communication process, the signal is transmitted through the channel and will be interfered by the noise to some extent. Therefore, when ciphertext images are transmitted through channels, they will inevitably be interfered with. The most common one is pepper and salt noise. Fig. 22 shows the decrypted image of R channel ciphertext images under different intensity of pepper and salt noise interference. It can be seen intuitively that although the decrypted image has some distortion, it has little effect on obtaining effective information, so the new system can resist the attack of noise to some extent.

FIGURE 22. Decrypted image disturbed by salt-and-pepper noise: (a)noise density $n = 0$, (b)noise density $n = 0.05$, (c)noise density $n = 0.1$, (d)noise density $n = 0.2$.

VII. CONCLUSION AND DISCUSSIONS

When a periodic tangent function is introduced in a memristive system, a new chaotic case is found where infinite lines of equilibria are coined which may be responsible for intermittent chaos. Numerical analysis and circuit simulation by PSpice show consistence with each other proving the new phenomenon. Most strikingly, the unique chaotic case shows hypermultistabiltiy with infinite uncountable different attractors and attractor self-reproducing with infinite countable ones. As a typical application, the property of image encryption is exhaustedly analyzed. With the chaotic signal from the new system, a color image is well encrypted and decrypted in key space. Histogram and correlation of adjacent pixels are used for showing the high encryption performance.

REFERENCES

[1] L. Wan and J. Sun, "Global asymptotic stability of Cohen–Grossberg neural network with continuously distributed delays," *Phys. Lett. A*, vol. 342, no. 4, pp. 331–340, Jul. 2005.

[2] L. Xiong, Y. Lu, Y. Zhang, and X. Zhang, "A novel memductor-based chaotic system and its applications in circuit design and experimental validation," *Complexity*, vol. 2019, pp. 1–17, Jan. 2019.

[3] W. Yao, C. Wang, J. Cao, Y. Sun, and C. Zhou, "Hybrid multisynchronization of coupled multistable memristive neural networks with time delays," *Neurocomputing*, vol. 363, pp. 281–294, Oct. 2019.

[4] J. Sun, G. Han, Z. Zeng, and Y. Wang, "Memristor-based neural network circuit of full-function pavlov associative memory with time delay and variable learning rate," *IEEE Trans. Cybern.*, vol. 50, no. 7, pp. 2935–2945, Jul. 2020.

[5] Z. Shi, S. Bi, H. Zhang, R. Lu, and X. S. Shen, "Improved auxiliary particle filter-based synchronization of chaotic colpitts circuit and its application to secure communication," *Wireless Commun. Mobile Comput.*, vol. 15, no. 10, pp. 1456–1470, Jul. 2015.

[6] F. Min, C. Li, L. Zhang, and C. Li, "Initial value-related dynamical analysis of the memristor-based system with reduced dimensions and its chaotic synchronization via adaptive sliding mode control method," *Chin. J. Phys.*, vol. 58, pp. 117–131, Apr. 2019.

[7] X. Zhang and C. Wang, "A novel multi-attractor period multi-scroll chaotic integrated circuit based on CMOS wide adjustable CCCII," *IEEE Access*, vol. 7, pp. 16336–16350, 2019.

[8] C. S. Hsu, "Global analysis of dynamical systems using posets and digraphs," *Int. J. Bifurcation Chaos*, vol. 5, no. 4, pp. 1085–1118, Aug. 1995.

[9] A. Akgul, I. Moroz, I. Pehlivan, and S. Vaidyanathan, "A new four-scroll chaotic attractor and its engineering applications," *Optik*, vol. 127, no. 13, pp. 5491–5499, Jul. 2016.

[10] A. Akgul, C. Arslan, and B. Aricioglu, "Design of an interface for random number generators based on integer and fractional order chaotic systems," *Chaos Theory Appl.*, vol. 1, no. 1, pp. 1–18, 2019.

[11] C. Li and J. C. Sprott, "Amplitude control approach for chaotic signals," *Nonlinear Dyn.*, vol. 73, no. 3, pp. 1335–1341, Aug. 2013.

[12] C. Li and J. C. Sprott, "Finding coexisting attractors using amplitude control," *Nonlinear Dyn.*, vol. 78, no. 3, pp. 2059–2064, Nov. 2014.

[13] C. Li, J. C. Sprott, A. Akgul, H. H. C. Iu, and Y. Zhao, "A new chaotic oscillator with free control," *Chaos*, vol. 27, no. 8, Aug. 2017, Art. no. 083101.

[14] C. Li, J. C. Sprott, Y. Liu, Z. Gu, and J. Zhang, "Offset boosting for breeding conditional symmetry," *Int. J. Bifurcation Chaos*, vol. 28, no. 14, 2019, Art. no. 1850163.

[15] J. Sun, Y. Wu, G. Cui, and Y. Wang, "Finite-time real combination synchronization of three complex-variable chaotic systems with unknown parameters via sliding mode control," *Nonlinear Dyn.*, vol. 88, no. 3, pp. 1677–1690, May 2017.

[16] G. Cheng, C. Wang, and H. Chen, "A novel color image encryption algorithm based on hyperchaotic system and permutation-diffusion architecture," *Int. J. Bifurcation Chaos*, vol. 29, no. 9, Aug. 2019, Art. no. 1950115.

[17] Z.-H. Gan, X.-L. Chai, D.-J. Han, and Y.-R. Chen, "A chaotic image encryption algorithm based on 3-D bit-plane permutation," *Neural Comput. Appl.*, vol. 31, no. 11, pp. 7111–7130, Nov. 2019.

[18] X. Chai, X. Fu, Z. Gan, Y. Lu, and Y. Chen, "A color image cryptosystem based on dynamic DNA encryption and chaos," *Signal Process.*, vol. 155, pp. 44–62, Feb. 2019.

[19] X. Chai, Z. Gan, K. Yuan, Y. Chen, and X. Liu, "A novel image encryption scheme based on DNA sequence operations and chaotic systems," *Neural Comput. Appl.*, vol. 31, no. 1, pp. 219–237, Jan. 2019.

[20] B. R. Andrievsky, N. V. Kuznetsov, G. A. Leonov, and A. Y. Pogromsky, "Hidden oscillations in aircraft flight control system with input saturation," *IFAC Proc. Volumes*, vol. 46, no. 12, pp. 75–79, 2013.

[21] G. A. Leonov, N. V. Kuznetsov, M. A. Kiseleva, E. P. Solovyeva, and A. M. Zaretskiy, "Hidden oscillations in mathematical model of drilling system actuated by induction motor with a wound rotor," *Nonlinear Dyn.*, vol. 77, nos. 1–2, pp. 277–288, Jul. 2014.

[22] G. A. Leonov, N. V. Kuznetsov, and T. N. Mokaev, "Homoclinic orbits, and self-excited and hidden attractors in a Lorenz-like system describing convective fluid motion," *Eur. Phys. J. Special Topics*, vol. 224, no. 8, pp. 1421–1458, Jul. 2015.

[23] H. Jiang, Y. Liu, Z. Wei, and L. Zhang, "Hidden chaotic attractors in a class of two-dimensional maps," *Nonlinear Dyn.*, vol. 85, no. 4, pp. 2719–2727, Sep. 2016.

[24] Z. Wei and W. Zhang, "Hidden hyperchaotic attractors in a modified Lorenz–Stenflo system with only one stable equilibrium," *Int. J. Bifurcation Chaos*, vol. 24, no. 10, Oct. 2014, Art. no. 1450127.

[25] V.-T. Pham, C. Volos, S. Jafari, Z. Wei, and X. Wang, "Constructing a novel no-equilibrium chaotic system," *Int. J. Bifurcation Chaos*, vol. 24, no. 5, May 2014, Art. no. 1450073.

[26] Q. Deng and C. Wang, "Multi-scroll hidden attractors with two stable equilibrium points," *Chaos*, vol. 29, no. 9, Sep. 2019, Art. no. 093112.

[27] B. C. Bao, J. P. Xu, and Z. Liu, "Initial state dependent dynamical behaviors in a memristor based chaotic circuit," *Chin. Phys. Lett.*, vol. 27, no. 7, pp. 51–53, 2010.

[28] C. Li and J. C. Sprott, "Coexisting hidden attractors in a 4-D simplified Lorenz system," *Int. J. Bifurcation Chaos*, vol. 24, no. 3, Mar. 2014, Art. no. 1450034.

[29] B. C. Bao, H. Bao, N. Wang, M. Chen, and Q. Xu, "Hidden extreme multistability in memristive hyperchaotic system," *Chaos, Solitons Fractals*, vol. 94, pp. 102–111, Jan. 2017.

[30] G. A. Leonov and N. V. Kuznetsov, "Hidden attractors in dynamical systems from hidden oscillations in Hilbert-Kolmogov, Aizerman, and Kalman problems to hidden chaotic attractors in Chua circuits," *Int. J. Bifurcation Chaos*, vol. 23, no. 4, 2013, Art. no. 1330002.

[31] G. A. Leonov, V. I. Vagaitsev, and N. V. Kuznetsov, "Localization of hidden Chua's attractors," *Phys. Lett. A*, vol. 375, no. 23, pp. 2230–2233, 2011.

[32] G. A. Leonov, N. V. Kuznetsov, and V. I. Vagaitsev, "Hidden attractor in smooth Chua systems," *Phys. D, Nonlinear Phenomena*, vol. 241, no. 18, pp. 1482–1486, Sep. 2012.

[33] X. Zhang and C. Wang, "Multiscroll hyperchaotic system with hidden attractors and its circuit implementation," *Int. J. Bifurcation Chaos*, vol. 29, no. 9, Aug. 2019, Art. no. 1950117.

[34] B.-C. Bao, M. Chen, H. Bao, and Q. Xu, "Extreme multistability in a memristive circuit," *Electron. Lett.*, vol. 52, no. 12, pp. 1008–1010, Jun. 2016.

[35] M. Molaie, S. Jafari, J. C. Sprott, and S. M. R. H. Golpayegani, "Simple chaotic flows with one stable equilibrium," *Int. J. Bifurcation Chaos*, vol. 23, no. 11, Nov. 2013, Art. no. 1350188.

[36] J. C. Sprott, X. Wang, and G. Chen, "Coexistence of point, periodic and strange attractors," *Int. J. Bifurcation Chaos*, vol. 23, no. 5, May 2013, Art. no. 1350093.

[37] P. Li, T. Zheng, C. Li, X. Wang, and W. Hu, "A unique jerk system with hidden chaotic oscillation," *Nonlinear Dyn.*, vol. 86, no. 1, pp. 197–203, Oct. 2016.

[38] S. Jafari, J. C. Sprott, and S. M. R. H. Golpayegani, "Elementary quadratic chaotic flows with no equilibria," *Phys. Lett. A*, vol. 377, no. 9, pp. 699–702, Mar. 2013.

[39] J. C. Sprott, "Strange attractors with various equilibrium types," *Eur. Phys. J. Special Topics*, vol. 224, no. 8, pp. 1409–1419, Jul. 2015.

[40] C. Li, J. C. Sprott, and W. Thio, "Bistability in a hyperchaotic system with a line equilibrium," *J. Experim. Theor. Phys.*, vol. 118, no. 3, pp. 494–500, Mar. 2014.

[41] S. Jafari and J. C. Sprott, "Simple chaotic flows with a line equilibrium," *Chaos, Solitons Fractals*, vol. 57, pp. 79–84, Dec. 2013.

[42] H. Bao, N. Wang, B. Bao, M. Chen, P. Jin, and G. Wang, "Initial condition-dependent dynamics and transient period in memristor-based hypogenetic jerk system with four line equilibria," *Commun. Nonlinear Sci. Numer. Simul.*, vol. 57, pp. 264–275, Apr. 2018.

[43] J. Sun, X. Zhao, J. Fang, and Y. Wang, "Autonomous memristor chaotic systems of infinite chaotic attractors and circuitry realization," *Nonlinear Dyn.*, vol. 94, no. 4, pp. 2879–2887, 2018.

[44] C. Hens, S. K. Dana, and U. Feudel, "Megastability: Coexistence of a countable infinity of nested attractors in a periodically-forced oscillator with spatially-periodic damping," *Chaos*, vol. 25, no. 5, Art. no. 053112, 2015.

[45] Q. Lai, Z. Wan, P. D. K. Kuate, and H. Fotsin, "Coexisting attractors, circuit implementation and synchronization control of a new chaotic system evolved from the simplest memristor chaotic circuit," *Commun. Nonlinear Sci. Numer. Simul.*, vol. 89, Oct. 2020, Art. no. 105341.

[46] Q. Lai, P. D. K. Kuate, F. Liu, and H. H.-C. Iu, "An extremely simple chaotic system with infinitely many coexisting attractors," *IEEE Trans. Circuits Syst. II, Exp. Briefs*, vol. 67, no. 6, pp. 1129–1133, Jun. 2020.

[47] J. C. Sprott, S. Jafari, A. J. M. Khalaf, and T. Kapitaniak, "Extreme multistability in a memristor-based multi-scroll hyper-chaotic system," *Eur. Phys. J. Special Topics*, vol. 226, no. 9, pp. 1979–1985, 2017.

[48] R. Karthikeyan, S. Çiçek, V.-T. Pham, A. Akgul, and P. Duraisamy, "A class of unexcited hyperjerk systems with megastability and its analog and microcontroller-based embedded system design," *Phys. Scripta*, vol. 95, no. 5, May 2020, Art. no. 055214.

[49] C. Li and J. C. Sprott, "An infinite 3-D quasiperiodic lattice of chaotic attractors," *Phys. Lett. A*, vol. 382, no. 8, pp. 581–587, Feb. 2018.
[50] C. Li, J. C. Sprott, W. Hu, and Y. Xu, "Infinite multistability in a self-reproducing chaotic system," *Int. J. Bifurcation Chaos*, vol. 27, no. 10, Sep. 2017, Art. no. 1750160.
[51] A. Akgul, H. Calgan, I. Koyuncu, I. Pehlivan, and A. Istanbullu, "Chaos-based engineering applications with a 3D chaotic system without equilibrium points," *Nonlinear Dyn.*, vol. 84, no. 2, pp. 481–495, Apr. 2016.
[52] S. Mobayen, C. K. Volos, S. Kaçar, Ü. Çavuşoğlu, and B. Vaseghi, "A chaotic system with infinite number of equilibria located on an exponential curve and its chaos-based engineering application," *Int. J. Bifurcation Chaos*, vol. 28, no. 9, Aug. 2018, Art. no. 1850112.
[53] X. X. Ai, K. H. Sun, S. B. He, and H. H. Wang, "Design and application of multi-scroll chaotic attractors based on simplified Lorenz system," *Acta Phys. Sinica*, vol. 63, no. 12, 2014, Art. no. 120511.
[54] C. Li and J. C. Sprott, "Variable-boostable chaotic flows," *Optik*, vol. 127, no. 22, pp. 10389–10398, Nov. 2016.

JIAYU SUN is currently pursuing the master's degree in information and communication engineering with the Nanjing University of Information Science and Technology, China. Her current research interests include memristive systems, chaotic circuits, and their applications.

CHUNBIAO LI (Member, IEEE) received the master's and Ph.D. degrees in succession from the Nanjing University of Science and Technology, in 2004 and 2009, respectively.

From 2010 to 2014, he was a Postdoctoral Fellow with the School of Information Science and Engineering, Southeast University. From 2012 to 2013, he was a Visiting Scholar with the Department of Physics, University of Wisconsin–Madison. He is currently a Professor with the School of Electronic and Information Engineering, Nanjing University of Information Science and Technology. His research interests include nonlinear dynamics and memristive circuits, including nonlinear circuits, systems, and corresponding applications. He has received several awards for his teaching and research in Jiangsu.

TIANAI LU is currently pursuing the master's degree in information and communication engineering with the Nanjing University of Information Science and Technology, China. His research interests include nonlinear dynamics and memristive circuits, including nonlinear circuits, systems, and corresponding applications.

AKIF AKGUL (Member, IEEE) received the B.Sc. degree in electronics-computer education from Kocaeli University, in 2009, the B.Sc. degree in electrical-electronics engineering from Sakarya University, in 2013, and the M.S. and Ph.D. degrees in electronics computer education and electrical-electronics engineering from Sakarya University, in 2011 and 2015, respectively. He joined the Institute of Electronics, Communications and Information Technology (ECIT), Queen's University Belfast, U.K., as a Visiting Researcher, in 2015. His current interests include analog electronics, chaos theory, chaotic systems, chaos-based engineering applications (cryptography, steganography, and pseudo and true random number generators), experimental chaotic synchronization, analysis and design of analog circuits, and microcomputer-based applications.

FUHONG MIN received the master's degree from the School of Communication and Control Engineering, Jiangnan University, in 2003, and the Ph.D. degree from the School of Automation, Nanjing University of Science and Technology, in 2007.

From 2009 to 2010, she was a Postdoctoral Fellow with the School of Mechanical Engineering, University of Southern Illinois. She is currently a Professor with the School of Electrical and Automation Engineering, Nanjing Normal University. Her research interests include memristive circuits, control and synchronization of chaotic circuits, and complex behavior of nonlinear power electronic circuits.